2019 IEEE 58th Conference on Decision and Control (CDC)
Palais des Congrès et des Expositions Nice Acropolis
Nice, France, December 11-13, 2019

Energy Shaping Control with Virtual Spring and Damper for Powered Exoskeletons

Jianping Lin, Nikhil Divekar, Ge Lv, *Member, IEEE*, and Robert D. Gregg, *Senior Member, IEEE*

***Abstract*— Task-invariant feedback control laws for powered exoskeletons are preferred to assist human users across varying locomotor activities. This goal can be achieved with energy shaping methods, where certain nonlinear partial differential equations, i.e., matching conditions, must be satisfied to find the achievable dynamics. Based on the energy shaping methods, open-loop systems can be mapped to closed-loop systems with a desired analytical expression of energy. In this paper, the desired energy consists of modified potential energy that is well-defined and unified across different contact conditions along with the energy of virtual springs and dampers that improve energy recycling during walking. The human-exoskeleton system achieves the input-output passivity and Lyapunov stability during the whole walking period with the proposed method. The corresponding controller provides assistive torques that closely match the human torques of a simulated biped model and able-bodied human subjects' data.**

I. INTRODUCTION

Powered exoskeletons have been developed to serve as rehabilitative and assistive devices for human users. They can either enhance a healthy person's abilities or support a physically impaired person's activities of daily living by providing powered hip, knee, and/or ankle motions based on different control designs. Despite the promising results in gait rehabilitation, significant challenges remain in the control design. Most exoskeletons use trajectory-based control methods, for instance, the robot suit Hybrid Assistive Limb [1], ReWalk [2], Ekso Bionics [3], and the bilateral Wandercraft [4]. However, controllers based on pre-defined trajectories cannot adjust to continuously varying activities. In contrast, task-invariant control for powered exoskeletons is more desirable as it provides more flexibility in assisting humans in a continuum of activities despite the specific tasks and environment changes.

An energy shaping method can serve as the task-invariant control by altering the dynamic characteristics of the human body via the Euler-Lagrange equations, which have already seen success in applications of bipedal locomotion [5], [6]. These applications of the energy shaping methods satisfy the set of nonlinear partial differential equations (PDEs) corresponding to the matching conditions. With the obtained solution of the matching conditions, the feasible structure of the closed-loop system can be derived and provides flexibility to the design of suitable closed-loop Euler-Lagrange systems. Spong [7] proposed the method of controlled symmetries that reproduces passive limit cycles on arbitrary slopes. Lv et al. [8], [9] proposed task-invariant controllers for powered exoskeletons using potential energy shaping methods which provide virtual body-weight support (BWS) during the walking gait. The stability of the altered dynamical system is considered during the fully-actuated phase (i.e., flat foot contact). During the underactuated phases (i.e., heel contact and toe contact), the closed-loop potential energy in [8], [9] cannot be retrieved directly from the altered dynamical system and can only be approximated. In [10], we used a modified mass/inertia matrix and approximated potential energy to achieve further assistance during walking via total energy shaping. However, the controller based on the total energy shaping method requires complicated calculations of the inverse of the mass/inertia matrix. Similar to [8], [9], the stability proof for the closed-loop system is limited to the fully-actuated phase due to the lack of an analytical expression of potential energy. New energy-shaping methods are needed to resolve these challenges for task-invariant exoskeleton control.

As mentioned in [11], mechanical energy is largely conserved during biped walking due to the interchange between the kinetic energy and the gravitational potential energy. Based on [12], the center of mass (COM) of the body is lowered during the forward acceleration and raised during the forward deceleration in a step. Despite the complex dynamics during walking or running, the Spring-Loaded Inverted Pendulum (SLIP) model [13] is a good template that describes all locomotion modes and captures the essential walking characteristics. Based on this simple model, the energy is stored in the spring when the support leg is compressed to decelerate the downward motion of the COM, and the stored energy is returned to redirect the COM upwards and forwards when the body is lifted and accelerated. Advantages of the SLIP model include energy recycling, power amplification, and impulse attenuation [14].

Motivated by the essential characteristics of the SLIP model, we design an energy-shaping controller for the stance leg that satisfies the matching condition with a true modified potential energy (MPE) and virtual springs and dampers (VSD). This MPE is well-defined across different contact conditions, including underactuated ones. Therefore, the input-output passivity and Lyapunov stability about an equilibrium point of the altered dynamical system can be guaranteed during every contact conditions. Moreover, the

Asterisk indicates the corresponding author.
J. Lin, N. Divekar, and R. D. Gregg* are with the Robotics Institute, University of Michigan, Ann Arbor, MI 48109, USA. rgregg@ieee.org
G. Lv is with the Robotics Institute, Carnegie Mellon University, Pittsburgh, PA 15213, USA.

This work was supported by NSF Award CMMI-1652514 and 1949869. This work was also supported by a gift from The Philip R. Jonsson Foundation. R. D. Gregg holds a Career Award at the Scientific Interface from the Burroughs Wellcome Fund.

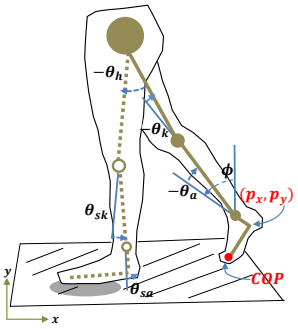

Fig. 1. Kinematic model of the human body. COP denotes the Center of Pressure. The solid links denote the stance leg, the dashed links denote the swing leg. This figure is reproduced from [16].

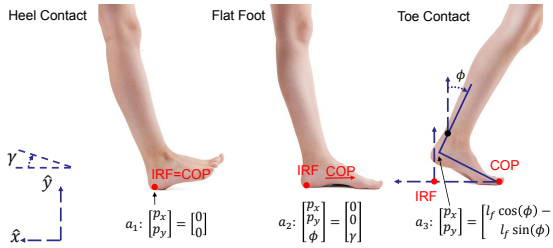

Fig. 2. Heel contact (left), flat foot (center), and toe contact conditions (right) during the single-support period of human locomotion. The biped is assumed to be walking on a slope with angle γ. This figure is reproduced from [9].

proposed controller based on the MPE and VSD provides assistive torques without taking the inverse of the mass/inertia matrix. The virtual springs also improve energy recycling during walking. Instead of simply adding linear torsion springs and dampers in the joints, we connect the hip and ankle joints, and the knee joint and the heel, with VSD to achieve a closed-loop system that considers the full dynamics of the biped over the specific kinematics of the joints.

The rest of this paper is organized as follows. In Section II, we review the concepts of the controlled Lagrangians and dynamics of the biped under different contact conditions. Feasible solutions of the matching condition with energy dissipation are derived and the MPE is proposed. The unified control law with VSD is shown in Section III, which also includes passivity and stability of the closed-loop system during the whole walking period. Simulation results based on different shaping strategies are given in Section IV. We test the unified control law on a simulated biped model and compare the torques between different shaping strategies. We also examine the torques provided by inputting able-bodied human subjects' kinematic data [15] into the controller, motivating future implementations in exoskeleton hardware. Finally, we present the conclusion in Section V.

II. Energy Shaping Methods for Powered Exoskeletons

In this section, we review the dynamics of the biped with stance and swing legs, separately. We also review the definition of energy shaping and the corresponding matching conditions. Based on the solution of the matching conditions, we propose the MPE shaping method to render a unified controller under different contact conditions.

A. Dynamics of the Biped

The biped model with coupled dynamics of the stance and swing legs is shown in Fig. 1. The masses of the human limb and the exoskeleton are combined together in the model. We assume identical powered knee-ankle exoskeletons on both human legs with no connection between them to make the full biped model symmetric [9], [17]. For control purposes, the dynamics of the stance and swing legs are modeled separately with coupled interaction forces. Consider the forced Euler-Lagrange system of the stance leg with the corresponding Lagrangian $L(q_{st}, \dot{q}_{st}) : TQ \to \mathbb{R}$ as

$$L(q_{st}, \dot{q}_{st}) = K(q_{st}, \dot{q}_{st}) - V(q_{st}) = \frac{1}{2}\dot{q}_{st}^T M(q_{st})\dot{q}_{st} - V(q_{st}),$$

where $q_{st} = (p_x, p_y, \phi, \theta_a, \theta_k)^T \in \mathbb{R}^{5\times 1}$ are the generalized coordinates in the 5-dimensional configuration space Q with (p_x, p_y) representing the Cartesian coordinates of the heel with respect to the inertial reference frame (IRF). The origin of the IRF is coincident with the stance heel during heel and flat foot contact. The heel angle ϕ is defined with respect to the vertical axis, and θ_a and θ_k are the stance ankle and knee angles, respectively. The kinetic energy $K(q_{st}, \dot{q}_{st})$ is based on the generalized mass/inertia matrix $M(q_{st}) \in \mathbb{R}^{5\times 5}$, and $V(q_{st}) \in \mathbb{R}$ is the potential energy. In the following equations, we omit the arguments q_{st} and $\dot{q}_{st}$ of the dynamic terms to abbreviate notation.

The dynamics of L with contact constraints are given as

$$\frac{\mathrm{d}}{\mathrm{dt}}\partial_{\dot{q}_{st}} L - \partial_{q_{st}} L + A_l^T \lambda = M\ddot{q}_{st} + C\dot{q}_{st} + N + A_l^T \lambda = \tau, \quad (1)$$

where C is the Coriolis matrix, and N is the gradient of the potential energy V along the generalized coordinates. We denote the human and exoskeleton torques as $\tau = \tau_{exo} + \tau_{hum} = Bu + Bv + J^T F$, where $B = [0_{2\times 3}, I_{2\times 2}]^T \in \mathbb{R}^{5\times 2}$ maps the human and exoskeleton inputs into the dynamics. The control input $u \in \mathbb{R}^{2\times 1}$ consists of the torques for ankle and knee provided by the exoskeleton and $v \in \mathbb{R}^{2\times 1}$ represents the human input for the same two joints. The interaction forces F between the hip and the swing thigh are mapped to the system by the body Jacobian matrix J. The Lagrange multiplier $\lambda \in \mathbb{R}^{w\times 1}$ represents the ground reaction forces and can be calculated as [18], [19]

$$\lambda = (A_l M^{-1} A_l^T)^{-1}[A_l M^{-1}(\tau - C\dot{q}_{st} - N) + \dot{A}_l \dot{q}_{st}].$$

The holonomic contact constraints of the biped can be expressed as $a_l(q_{st}) = 0_{w\times 1}$ where w denotes the number of constraints. The constraint matrix $A_l = \nabla_{q_{st}} a_l \in \mathbb{R}^{w\times 5}$ satisfies $A_l(q_{st})\dot{q}_{st} = 0$ with the subscript $l \in \{heel, flat, toe\}$ indicating the contact configurations shown in Fig. 2.

For the heel contact phase, the heel is fixed to the ground and the stance leg rotates about the heel. The holonomic

contact constraint is $a_{heel}(q_{st}) = (p_x, p_y)^T = 0$ and the matrix $A_{heel} = \nabla_{q_{st}} a_{heel} = [I_{2\times 2}, 0_{2\times 3}]$. At the flat foot phase, the foot is flat on the ground and ϕ is equal to the slope angle γ. The constraint is $a_{flat}(q_{st}) = (p_x, p_y, \phi - \gamma)^T = 0$ and the matrix $A_{flat} = [I_{3\times 3}, 0_{3\times 2}]$. During the toe contact phase, the stance leg rotates around the toe. The corresponding constraint is $a_{toe}(q_{st}) = (p_x - l_f \cos(\phi) + l_f, p_y - l_f \sin(\phi))^T = 0$ and the matrix A_{toe} is given as

$$A_{toe}(q_{st}) = \begin{bmatrix} 1 & 0 & l_f \sin(\phi) & 0 & 0 \\ 0 & 1 & -l_f \cos(\phi) & 0 & 0 \end{bmatrix}.$$

For the dynamical model of the swing leg, the generalized coordinates in the configuration space are given as $q_{sw} = (h_x, h_y, \theta_{th}, \theta_{sk}, \theta_{sa})^T \in \mathbb{R}^{5\times 1}$, where (h_x, h_y) are the positions of the hip with respect to the IRF, θ_{th} is the angle between the vertical axis and the swing thigh, and θ_{sk} and θ_{sa} are the swing knee and ankle angles, respectively. We do not have contact constraints in the swing leg dynamics, i.e., $A(q_{sw}) = 0$.

B. Solution of the Matching Conditions

We wish to achieve the closed-loop Lagrangian system of the stance leg with $\tilde{L} = \frac{1}{2}\dot{q}_{st}^T M \dot{q}_{st} - \tilde{V}$ as

$$M\ddot{q}_{st} + C\dot{q}_{st} + \tilde{N} + \nabla_{\dot{q}_{st}} D + A_l^T \lambda = Bv + J^T F, \qquad (2)$$

where $\tilde{N} = \nabla_{q_{st}} \tilde{V} \in \mathbb{R}^{5\times 1}$ represents the closed-loop potential forces vector, and $D : TQ \to \mathbb{R}_{\geqslant 0}$ represents some positive semi-definite dissipation functions of $(q_{st}, \dot{q}_{st})$. We treat the ground reaction forces $A_l^T \lambda$ as the external forces, which remain unchanged in the closed-loop system. According to [20], systems (1) and (2) match if and only if there exists a full rank left annihilator of B in the orthogonal projection form, i.e., $B^\perp B = 0$, for all $q_{st} \in Q$ such that

$$\begin{aligned} 0 &= B^\perp M[M^{-1}(C\dot{q}_{st} + N + A_l^T\lambda - Bv - J^T F) \\ &\quad - M^{-1}(C\dot{q}_{st} + \tilde{N} + \nabla_{\dot{q}_{st}} D + A_l^T \lambda - Bv - J^T F)], \\ &= B^\perp (N - \tilde{N} - \nabla_{\dot{q}_{st}} D), \end{aligned} \qquad (3)$$

holds true along all trajectories $(q_{st}, \dot{q}_{st}) \in TQ$ [5]. The corresponding state feedback control law is explicitly given by

$$u = (B^T B)^{-1} B^T (N - \tilde{N} - \nabla_{\dot{q}_{st}} D). \qquad (4)$$

Equation (3) is a simplified matching condition without the modified mass/inertia matrix in two unknowns $\tilde{V}$ and $\nabla_{\dot{q}_{st}} D$. The human joint input v and the interaction forces F are generally difficult to measure in practice. Together with the ground reaction forces $A_l^T \lambda$, these terms are treated as external forces and not changed in the closed-loop system, so that they disappear in the matching condition. As a result, the control law (4) does not depend on the human joint input, the interaction forces, or the environmental reaction forces, making it task-invariant and unified with respect to different contact conditions.

The left annihilator matrix $B^\perp$ in the stance leg model is given as

$$B^\perp = \begin{bmatrix} I_{3\times 3} & 0_{3\times 2} \\ 0_{2\times 3} & 0_{2\times 2} \end{bmatrix}.$$

Based on the matrix $B^\perp$, we can express equation (3) as

$$0 = B^\perp [N - \tilde{N} - \nabla_{\dot{q}_{st}} D] = \begin{bmatrix} N_{1:3} - \tilde{N}_{1:3} - \nabla_{\dot{q}_{st}} D_{1:3} \\ 0_{2\times 1} \end{bmatrix},$$

where $N_{1:3} \in \mathbb{R}^{3\times 1}$ represents the first three elements of the vector N. To satisfy the matching condition, the first three rows of $\tilde{N}$ must be equal to those of N, while D must be a function that only depends on $\dot{\theta}_a$ and $\dot{\theta}_k$. As a result, the closed-loop potential force vector is given as $\tilde{N} = [\tilde{N}_{1:3}^T, \tilde{N}_{4:5}^T]^T = [N_{1:3}^T, N_{4:5}^T + \hat{N}^T]^T$ with free parameters $\hat{N} \in \mathbb{R}^{2\times 1}$, and the dissipation force vector is given as $\nabla_{\dot{q}_{st}} D = [0_{1\times 3}, \nabla_{\dot{\theta}_a} D, \nabla_{\dot{\theta}_k} D]^T$.

C. MPE Shaping Method for Powered Exoskeletons

Our prior work [10] of potential energy shaping reduce the gravitational forces vector by setting $\hat{N} = (\mu - 1) N_{4:5}$ with a constant $\mu \in [0, 1]$ [10]. As a result, the torques acting on the ankle and knee joints due to gravity are reduced. The potential energy $\tilde{V}$ is well defined during the fully-actuated phase, i.e., the flat foot contact, while during the under-actuated phases, i.e., the heel contact and toe contact, $\tilde{V}$ cannot be retrieved directly from the altered dynamical system and is only approximated. As a result, the stability proof of the closed-loop system is limited to the fully-actuated phase. In order to get a well-defined potential energy $\tilde{V}$ over the whole walking period, we investigate the structure of the gravitational forces vector.

The gravitational force vector of the stance leg is given by $N(q_{st}) = [N_{1:3}^T, N_4, N_5]^T$, where

$$\begin{aligned} N_5 &= -\frac{1}{2} g l_t (M_t + 2M_p) \sin(\phi + \theta_a + \theta_k), \\ N_4 &= -\frac{1}{2} g l_s (M_s + 2M_t + 2M_p) \sin(\phi + \theta_a) + N_5, \end{aligned}$$

where M_s, M_t, and M_p represent the mass of the shank, thigh, and hip, respectively, and l_s and l_t represent the length of the shank and thigh, respectively. The components of N_4 and N_5 consist of the torques acting on the ankle and knee joints generated by the gravity forces. We can decompose N_5 in the following form

$$N_5 = -\frac{1}{2} \begin{bmatrix} g(M_t + 2M_p)\cos(\phi) \\ g(M_t + 2M_p)\sin(\phi) \end{bmatrix}^T \begin{bmatrix} l_t \sin(\theta_a + \theta_k) \\ l_t \cos(\theta_a + \theta_k) \end{bmatrix}.$$

As illustrated in Fig. 3, the gravitational force acting on the mass of thigh can be decomposed into two components, where one is acting parallel to the foot plane, i.e., $M_t g \sin(\phi)$, and the other is acting perpendicular to the foot plane, i.e., $M_t g \cos(\phi)$. The products of these two components with the distances from knee joint formulate the torques related to M_t in N_5. We treat the torques related to M_p in N_5 similarly.

The MPE shaping method focuses on reducing the torques provided by the forces acting perpendicular to the foot based on the assumption that $\phi \in [-\frac{\pi}{2}, \frac{\pi}{2}]$ (for the swing leg, $\theta_{th} \in [-\frac{\pi}{2}, \frac{\pi}{2}]$), so that $\cos(\phi)$ is always positive in the configuration space Q. This assumption is reasonable and covers the vast majority of human locomotion modes [15].

Consequently, we can have $\tilde{N}_5 = N_5 + \hat{N}_5$, and $\tilde{N}_4 = N_4 + \hat{N}_4$, where

$$\hat{N}_5 = -\mu_2 \frac{1}{2} g l_t (M_t + 2M_p) \sin(\theta_a + \theta_k),$$
$$\hat{N}_4 = -\mu_1 \frac{1}{2} g l_s (M_s + 2M_t + 2M_p) \sin(\theta_a) + \hat{N}_5.$$

The constant coefficients μ_2 and μ_1 determine the quantity of reduced torques acting on ankle and knee joints and give us choices on providing further/less assistance on either ankle or knee joints. As a result, the gravitational forces vector in the closed-loop system is given by $\tilde{N} = [N_{1:3}^T, N_{4:5}^T + \hat{N}^T]^T$, with $\hat{N} = [\hat{N}_4, \hat{N}_5]^T$, which is well-defined with a symmetric Jacobian matrix, i.e., $\frac{\partial \tilde{N}_i}{\partial q_j} = \frac{\partial \tilde{N}_j}{\partial q_i}$ for any $i, j \in \{1, \cdots, 5\}$. The corresponding potential energy in the closed-loop system can then be retrieved by the variable gradient method [21], even during the underactuated phases. The MPE in the closed-loop system for the swing leg is defined similarly to the stance leg except that the gravitational forces are decomposed into two components that are parallel and perpendicular to the thigh.

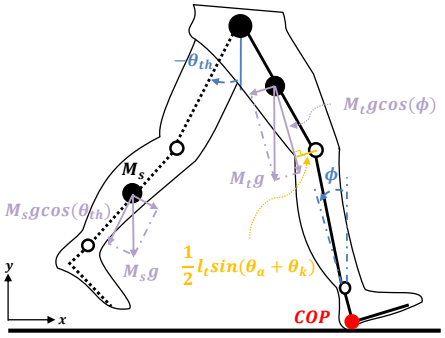

Fig. 3. For the stance leg, the gravitational force acting on the knee joint can be decomposed into two components that are parallel and perpendicular to the foot. The stance leg is shown in solid black and the swing leg in dashed black.

III. Unified Controller with VSD

In this section, we design the unified controller based on the energy shaping methods which consist of MPE and VSD. The virtual stiffness and damping constants are properly chosen to be applicable to the physical system. The corresponding control law satisfies the matching condition and the input-output passivity. We also show possible stability results with certain assumptions on the form of human input.

A. VSD for Powered Exoskeletons

As mentioned before, the dynamics of the walking gait can be simplified as a SLIP model with the legs modeled as spring-loaded massless straight links. Motivated by the SLIP template, our desired closed-loop energy contains additional virtual elastic potential (spring) and dissipation (damper) energy to achieve energy recycling. As shown in Fig. 4, we add a spring and damper system across the hip and ankle joints, as well as a spring and damper system across the knee joints and the heel.

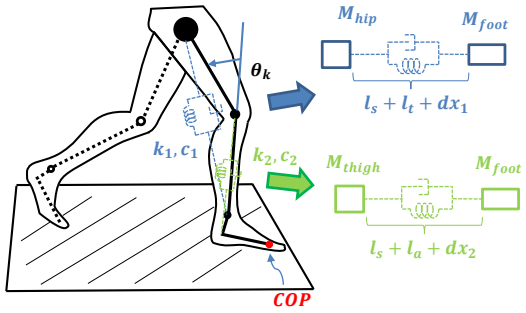

Fig. 4. Model of the stance leg with VSD connecting the ankle and hip joints, and the knee joint and the heel.

The displacement x_1 that represents the distance between the hip and ankle joints can be written as a function of the knee angle θ_k, i.e.,

$$x_1 = f(\theta_k) = l_s + l_t - [l_s^2 + l_t^2 + 2 l_s l_t \cos(\theta_k)]^{\frac{1}{2}}.$$

The displacement x_2 that represents the distance between the knee joint and the heel is given as

$$x_2 = g(\theta_a) = l_s + l_a - [l_s^2 + l_a^2 + 2 l_s l_a \cos(\theta_a)]^{\frac{1}{2}}.$$

As a result, the virtual spring energy is $V_s = \sum_{i=1}^{2} \frac{1}{2} k_i x_i^2 = \frac{1}{2}(k_1 f(\theta_k)^2 + k_2 g(\theta_a)^2)$ and the dissipation function of the damper is $D = \sum_{i=1}^{2} \frac{1}{2} c_i \dot{x}_i^2 = \frac{1}{2} c_1 [\frac{\partial f(\theta_k)}{\partial \theta_k} \dot{\theta}_k]^2 + \frac{1}{2} c_2 [\frac{\partial g(\theta_a)}{\partial \theta_a} \dot{\theta}_a]^2$. Since the additional elastic potential and dissipation energy depend only on θ_k, $\dot{\theta}_k$, θ_a, and $\dot{\theta}_a$, the corresponding $\tilde{N} + \nabla_{q_{st}} V_s$ and $\nabla_{\dot{q}_{st}} D$ in the closed-loop system is within the specification given in Section II-B, i.e., the matching condition is satisfied.

The application of adding VSD connecting two joints are different from simply adding linear torsion springs and dampers in the joints, where the torques provided by linear torsion springs and dampers are given by $K_p(q - q_0)$ and $K_d \dot{q}$, i.e., PD controllers with constant K_p and K_d. Based on our model, the closed-loop system considers the full dynamics of the biped over the specific kinematics of the joints. The Lagrange of the closed-loop system becomes $\tilde{L} = \frac{1}{2} \dot{q}_{st}^T M \dot{q}_{st} + \tilde{V} + V_s$ with dissipation function $D > 0$, and the corresponding dynamics of the system is given as

$$M \ddot{q}_{st} + C \dot{q}_{st} + \tilde{N} + N_s + \nabla_{\dot{q}_{st}} D + A_l^T \lambda = \tau_{hum}, \qquad (5)$$

where $N_s = \nabla_{q_{st}} V_s$ represents the force vector corresponding to the spring energy. The unified controller across different contact conditions is based on the energy shaping methods which consist of MPE and VSD.

B. Passivity and Stability of the Closed-Loop System with VSD

Considering the closed-loop system (5), the passive relationship from the human input τ_{hum} to the output $\dot{q}_{st}$ can be proved by choosing the total energy $E(q_{st}, \dot{q}_{st}) = \frac{1}{2} \dot{q}_{st}^T M \dot{q}_{st} + \tilde{V} + V_s > 0$ as the storage function. Therefore,

the time derivative of $E(q_{st},\dot{q}_{st})$ is

$$\begin{aligned}\dot{E}(q_{st},\dot{q}_{st}) &= \dot{q}_{st}^T(M\ddot{q}_{st}+\frac{1}{2}\dot{M}\dot{q}_{st}+\tilde{N}+N_s)\\ &= \dot{q}_{st}^T(-C\dot{q}_{st}+\frac{1}{2}\dot{M}\dot{q}_{st}-\nabla_{\dot{q}_{st}}D-A_l^T\lambda+\tau_{hum})\\ &= -c_1[\partial_{\theta_k}f(\theta_k)\dot{\theta}_k]^2-c_2[\partial_{\theta_a}g(\theta_a)\dot{\theta}_a]^2+\dot{q}_{st}^T\tau_{hum}\\ &\leqslant \dot{q}_{st}^T\tau_{hum},\end{aligned}$$

where $\dot{M}-2C$ is skew-symmetric and $\dot{q}_{st}^TA_l^T\lambda=0$ due to the fact that constraint forces do no work [18].

The stability of the closed-loop system around the equilibrium point $(q_{st}^\star,0)$ can also be proved where $(q_{st}^\star,0)$ is the state that $\tilde{N}+N_s+A_l^T\lambda-\tau_{hum}=0$, i.e., the forces along the shaped potential energy balance the muscular spring forces and the ground reaction forces. We assume that the human is modulating joint impedance where $\tau_{hum}=-K_pe-K_d\dot{e}$ [9]. The constant diagonal matrices $K_p,\ K_d\in\mathbb{R}^{5\times5}$ are positive semi-definite and $e=q_{st}-\bar{q}_{st}$ represents the difference between q_{st} and the fixed constant vector $\bar{q}_{st}$. We can set the Lyapunov function to be $\mathscr{V}(q_{st},\dot{q}_{st})=E+\frac{1}{2}e^TK_pe+\int_{q_0}^{q_{st}}A_l(s)^T\lambda(s,0)\cdot\mathrm{d}s-\bar{\mathscr{V}}$ where q_0 is the state at $t=0$ and $\bar{\mathscr{V}}$ is a constant such that $\bar{\mathscr{V}}=E(q_{st}^\star,0)+\frac{1}{2}(q_{st}^\star-\bar{q}_{st})^TK_p(q_{st}^\star-\bar{q}_{st})$.

Lemma 3.1: The Lyapunov function $\mathscr{V}(q_{st},\dot{q}_{st})$ is positive definite around the equilibrium point with $\mathscr{V}(q_{st}^\star,0)=0$ in the tangent bundle TQ.

Proof: The Lyapunov function $\mathscr{V}(q_{st},\dot{q}_{st})$ achieves the minimum value at $\partial_{q_{st}}\mathscr{V}=0$ and $\partial_{\dot{q}_{st}}\mathscr{V}=0$. Given $\partial_{\dot{q}_{st}}\mathscr{V}=0$, we have $\dot{q}_{st}=0$, and given $\partial_{q_{st}}\mathscr{V}=0$, we have

$$\partial_{q_{st}}\mathscr{V}(q_{st},0)=\tilde{N}+N_s+K_pe+A_l^T\lambda=0,$$

which corresponds to the equilibrium point $(q_{st}^\star,0)$. Since $(q_{st}^\star,0)$ achieves the minimal value of $\mathscr{V}(q_{st},\dot{q}_{st})$, by subtracting $\bar{\mathscr{V}}$, we have $\mathscr{V}(q_{st}^\star,0)=0$. For any $(q,\dot{q})\in TQ$ with $(q,\dot{q})\neq(q_{st}^\star,0)$, we have

$$\begin{aligned}\mathscr{V}(q_{st},\dot{q}_{st}) &= \frac{1}{2}\dot{q}_{st}^TM\dot{q}_{st}+\tilde{V}+V_s+\frac{1}{2}e^TK_pe\\ &\quad+\int_{q_0}^{q_{st}}A_l(s)^T\lambda(s,0)\cdot\mathrm{d}s-\bar{\mathscr{V}}\\ &= \frac{1}{2}\dot{q_{st}}^TM\dot{q}_{st}+\tilde{V}+V_s+\frac{1}{2}e^TK_pe-\bar{\mathscr{V}}>0,\end{aligned}$$

where $\int_{q_0}^{q_{st}}A_l(s)^T\lambda(s,0)\cdot\mathrm{d}s=0$ due to the fact that $A_l^T\lambda\cdot dq_{st}=0$ [18]. The incorporation of $\int_{q_0}^{q_{st}}A_l(s)^T\lambda(s,0)\cdot ds$ guarantees the appearance of the GRFs to balance the unactuated parts of $\tilde{N}$ at the equilibrium state when $\partial_{q_{st}}\mathscr{V}(q_{st},0)=0$. ∎

Having verified that $\mathscr{V}$ is a proper Lyapunov function, we take the time derivative of $\mathscr{V}$ to obtain

$$\begin{aligned}\dot{\mathscr{V}}(q_{st},\dot{q}_{st}) &= -c_1[\partial_{\theta_k}f(\theta_k)\dot{\theta}_k]^2-c_2[\partial_{\theta_a}g(\theta_a)\dot{\theta}_a]^2\\ &\quad+\dot{q}_{st}^T\tau_{hum}+\dot{q}_{st}^TK_pe\\ &\leqslant \dot{q}_{st}^T(-K_pe-K_d\dot{e})+\dot{q}_{st}^TK_pe\leqslant 0,\end{aligned}$$

which implies the Lyapunov stability of the closed-loop system at the equilibrium point. Based on LaSalle's theorem [21], $\dot{\mathscr{V}}\equiv0$ implies $\ddot{q}_{st}=\dot{q}_{st}\equiv0$, so that $\mathscr{V}(q_{st},\dot{q}_{st})$ only vanishes at the equilibrium point $(q_{st}^\star,0)$ and the closed-loop system is asymptotically stable. The input-output passivity and stability of the closed-loop system for the swing leg can be proved similarly without the constraint matrix A.

IV. Simulations and Experimental Results

In this section, we specify the system parameters to be applied in the simulation and introduce the simulation method. We compare the results based on different shaping strategies.

A. System Parameters and Simulation Methods

As mentioned in Section II-A, we assume that we have identical powered knee-ankle exoskeletons on both human legs. As a result, the corresponding controllers (4) for both legs only require local feedback and depend on the dynamical models of the stance and swing legs, respectively. In the simulation, the exoskeleton controller is applied to an 8-DOF human-like biped where the coupled dynamics of the two legs are shown in Fig. 1. We assume there is no continuous double-support period during walking of the biped model in the simulation. The generalized coordinates of the full biped model in the configuration space are given as $q=(p_x,p_y,\phi,\theta_a,\theta_k,\theta_h,\theta_{sk},\theta_{sa})^T\in\mathbb{R}^{8\times1}$, where θ_h represents the hip angle between the stance and swing thigh. The full biped is modeled as a hybrid dynamical system where impacts happen at the change of contact conditions [9], [17]. We simulate the full biped with joint impedance control for the human muscular inputs [22]. The human impedance parameters $\bar{q}_{st}$, K_p, and K_d are kept constant with respect to each phase of stance and the model parameters are chosen from Table I in [9]. Based on the maximum allowable torques provided by exoskeletons, we set the feasible VSD constants to be $k_1=400\ N/m,\ c_1=200\ N\cdot s/m$, and $k_2=20000\ N/m,\ c_2=1000\ N\cdot s/m$.

B. Simulated Biped Model

We present the simulation results of three different shaping strategies: the MPE, the VSD, and the combination of MPE and VSD on a simulated biped model. The exoskeleton torques at the stance ankle and knee during one steady step for the three different shaping strategies are shown in Fig. 5. The constant coefficients of the MPE shaping methods in the simulation are set to $\mu_1=-0.15$ and $\mu_2=0.2\mu_1$. The swing leg controller for all three strategies is the same, i.e., the MPE shaping method with the same parameters μ_1 and μ_2. As a result, the torques of the swing leg controller are identical and are omitted from the results. The shape of torques generated by the MPE+VSD is similar to the human torques in the simulation. The VSD provide torques during the start of the step which helps absorb the impact energy and regulate the joint velocities.

Fig. 6 gives the simulated metabolic costs for different shaping strategies, where the metabolic cost estimate is defined in [23]. The metabolic cost is the sum of the individual joint costs for one step and reflects the energy consumption of the muscles to generate forces [9]. All three

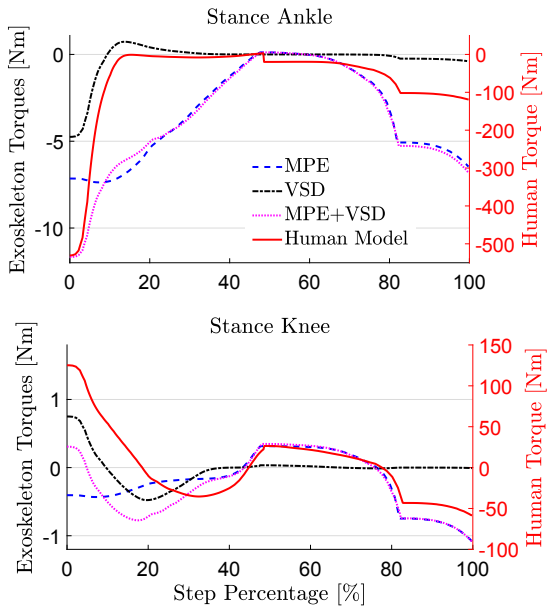

Fig. 5. The exoskeleton torques with different shaping strategies during one steady step are compared with the simulated human torques. Positive values represent ankle dorsiflexion torques and knee extension torques.

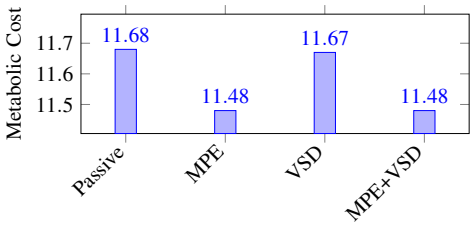

Fig. 6. The estimated metabolic costs with different shaping strategies.

shaping strategies have reduced metabolic costs. The VSD contributes a small reduction of the metabolic cost due to the small variations of joint angles and joint velocities in the simulation model.

C. Normative Kinematic Data

We examine the torques provided by inputting able-bodied human subjects' normative kinematic data [15] into the controller. Fig. 7 compares estimated exoskeleton joint torques with average able-bodied data from [15], for the decline, level and incline conditions, respectively. The damping constant c_1 in VSD is reduced to provide achievable torques from the exoskeleton, where $c_1 = 20\ N \cdot s/m$. The performance of the MPE and MPE+VSD strategies is compared to the potential energy shaping strategy in [8]. The main phases during stance when exoskeleton assistance is required are weight absorption and push-off [24]. A weakness in the quadriceps muscles results in knee-buckling during weight acceptance, which makes patients tend to adopt a locked-knee gait. Knee extension, as well as plantar flexion, is used in late stance to propel the body forwards and project the limb upwards (swing). The inability to push-off (from weakness in plantar-flexors and/or quadriceps) results in

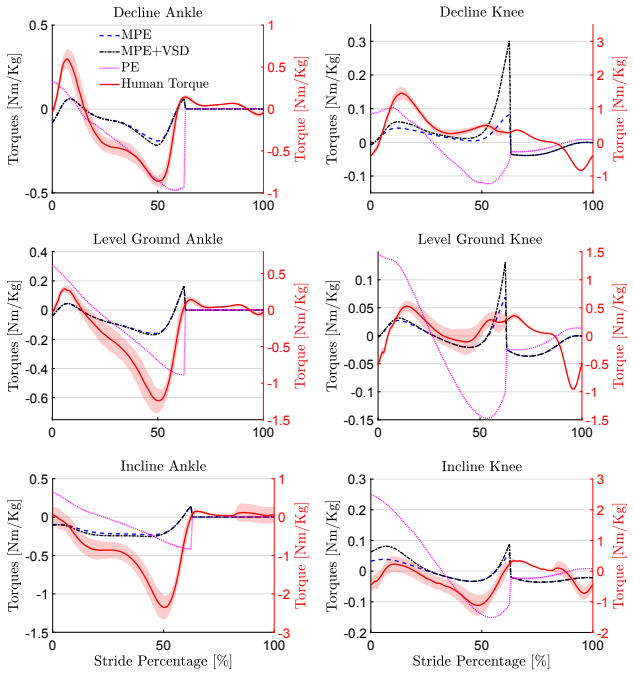

Fig. 7. From top to bottom: the torques acting on ankles and knees based on decline ($-10°$), level ground ($0°$), and incline ($10°$) walking on a treadmill with walking speed 1.2 m/s. The red solid lines represent the averaged human torques with variance. PE represents the potential energy shaping method introduced in [8]. Positive values represent ankle dorsiflexion torques and knee extension torques.

reduced walking speeds as well as reduced foot clearance [24]. It can be seen that the potential energy shaping strategy provides very aggressive plantar-flexion torques that increase in a linear fashion until the terminal stance. This can be dangerous as it can cause hyper plantar-flexion during the early swing and further aggravate the problem of foot-drop. The MPE and MPE+VSD strategies show a marked improvement in this regard, tapering down the plantar-flexion torques towards terminal stance. The drawback, however, may be the overall low plantar-flexion torques for level and incline conditions. The potential energy shaping strategy provides knee flexion torques in late stance for all conditions, which may be helpful for incline, but is counterproductive for the decline and level conditions. This is corrected with the MPE and MPE+VSD strategies, which provide the required knee extension torques (albeit excessively with MPE+VSD for decline). All three strategies in Fig. 7 provide the knee extension torques during weight absorption, however, the potential energy shaping strategy is overly aggressive in early stance.

V. CONCLUSIONS

In this paper, we designed a task-invariant feedback control law by using the energy shaping methods with MPE and VSD. Different from our prior work [10], the MPE shaping method is well-defined during all gait phases. We used the VSD to achieve further energy recycling and provide further assistance instead of taking the mass/inertia matrix inverse, which is beneficial for implementation purposes.

The open-loop system was mapped to a passive and stable closed-loop system based on the unified control law. Simulations were performed on different shaping strategies and the corresponding controllers were tested using able-bodied human subjects' kinematic data. Based on the simulation results, the proposed MPE + VSD method provided torques that closely match human torques in different tasks. This demonstrates the potential for this control strategy to assist patients in future experimental studies. We will also consider the passivity conditions where the physical damping in the mechanism should be sufficient to dissipate the excess energy due to the sampling in discrete-time control implementations in embedded systems as shown in [25]. The passivity conditions may limit the value of the spring and damping coefficients and affect the overall performance of the controller. In that scenario, we will investigate the interconnection and damping assignment passivity-based control (IDA-PBC) [26], [27], which is a more general methodology and provides extra flexibility for control design.

REFERENCES

[1] K. Suzuki, G. Mito, H. Kawamoto, Y. Hasegawa, and Y. Sankai, "Intention-based walking support for paraplegia patients with robot suit hal," *Advanced Robotics*, vol. 21, no. 12, pp. 1441–1469, 2007.

[2] G. Zeilig, H. Weingarden, M. Zwecker, I. Dudkiewicz, A. Bloch, and A. Esquenazi, "Safety and tolerance of the rewalk^{TM} exoskeleton suit for ambulation by people with complete spinal cord injury: a pilot study," *The journal of spinal cord medicine*, vol. 35, no. 2, pp. 96–101, 2012.

[3] S. A. Kolakowsky-Hayner, J. Crew, S. Moran, and A. Shah, "Safety and feasibility of using the eksotm bionic exoskeleton to aid ambulation after spinal cord injury," *J Spine*, vol. 4, p. 003, 2013.

[4] O. Harib, A. Hereid, A. Agrawal, T. Gurriet, S. Finet, G. Boeris, A. Duburcq, M. E. Mungai, M. Masselin, A. D. Ames, *et al.*, "Feedback control of an exoskeleton for paraplegics: Toward robustly stable, hands-free dynamic walking," *IEEE Control Systems Magazine*, vol. 38, no. 6, pp. 61–87, 2018.

[5] A. M. Bloch, N. E. Leonard, and J. E. Marsden, "Stabilization of mechanical systems using controlled lagrangians," in *Decision and Control, 1997., Proceedings of the 36th IEEE Conference on*, vol. 3. IEEE, 1997, pp. 2356–2361.

[6] R. Ortega, J. A. L. Perez, P. J. Nicklasson, and H. J. Sira-Ramirez, *Passivity-based control of Euler-Lagrange systems: mechanical, electrical and electromechanical applications*. Springer Science & Business Media, 2013.

[7] M. W. Spong, "The passivity paradigm in the control of bipedal robots," in *International Conference on Climbing and Walking Robots*. Springer, 2005, pp. 775–786.

[8] G. Lv and R. D. Gregg, "Underactuated potential energy shaping with contact constraints: Application to a powered knee-ankle orthosis," *IEEE Transactions on Control Systems Technology*, vol. 26, no. 1, pp. 181–193, 2018.

[9] G. Lv, H. Zhu, and R. D. Gregg, "On the design and control of highly backdrivable lower-limb exoskeletons: A discussion of past and ongoing work," *IEEE Control Systems Magazine*, vol. 38, no. 6, pp. 88–113, 2018.

[10] J. Lin, G. Lv, and R. D. Gregg, "Contact-invariant total energy shaping for powered exoskeletons," in *Proceedings of the American Control Conference*. IEEE, 2019.

[11] G. Cavagna, F. Saibene, and R. Margaria, "External work in walking," *Journal of applied physiology*, vol. 18, no. 1, pp. 1–9, 1963.

[12] G. Cavagna, P. Willems, and N. Heglund, "The role of gravity in human walking: pendular energy exchange, external work and optimal speed," *The Journal of Physiology*, vol. 528, no. 3, pp. 657–668, 2000.

[13] H. Geyer, A. Seyfarth, and R. Blickhan, "Compliant leg behaviour explains basic dynamics of walking and running," *Proceedings of the Royal Society B: Biological Sciences*, vol. 273, no. 1603, pp. 2861–2867, 2006.

[14] S. Rezazadeh, A. Abate, R. L. Hatton, and J. W. Hurst, "Robot leg design: A constructive framework," *IEEE Access*, vol. 6, pp. 54 369–54 387, 2018.

[15] K. R. Embry, D. J. Villarreal, R. L. Macaluso, and R. D. Gregg, "Modeling the kinematics of human locomotion over continuously varying speeds and inclines," *IEEE transactions on neural systems and rehabilitation engineering*, vol. 26, no. 12, pp. 2342–2350, 2018.

[16] M. Yeatman, G. Lv, and R. D. Gregg, "Decentralized passivity-based control with a generalized energy storage function for robust biped locomotion," *Journal of Dynamic Systems, Measurement, and Control*, vol. 141, no. 10, p. 101007, 2019.

[17] H. Zhu, J. Doan, C. Stence, G. Lv, T. Elery, and R. Gregg, "Design and validation of a torque dense, highly backdrivable powered knee-ankle orthosis," in *Robotics and Automation (ICRA), 2017 IEEE International Conference on*. IEEE, 2017, pp. 504–510.

[18] R. M. Murray, *A mathematical introduction to robotic manipulation*. CRC press, 2017.

[19] R. D. Gregg, T. Lenzi, L. J. Hargrove, and J. W. Sensinger, "Virtual constraint control of a powered prosthetic leg: From simulation to experiments with transfemoral amputees," *IEEE Transactions on Robotics*, vol. 30, no. 6, pp. 1455–1471, 2014.

[20] G. Blankenstein, R. Ortega, and A. J. Van Der Schaft, "The matching conditions of controlled lagrangians and ida-passivity based control," *International Journal of Control*, vol. 75, no. 9, pp. 645–665, 2002.

[21] H. K. Khalil and J. Grizzle, *Nonlinear systems*. Prentice hall Upper Saddle River, NJ, 2002, vol. 3.

[22] D. J. Braun, J. E. Mitchell, and M. Goldfarb, "Actuated dynamic walking in a seven-link biped robot," *IEEE/ASME Transactions on Mechatronics*, vol. 17, no. 1, pp. 147–156, 2012.

[23] A. E. Martin and J. P. Schmiedeler, "Predicting human walking gaits with a simple planar model," *Journal of biomechanics*, vol. 47, no. 6, pp. 1416–1421, 2014.

[24] J. Boudarham, R. Zory, F. Genet, G. Vigné, D. Bensmail, N. Roche, and D. Pradon, "Effects of a knee–ankle–foot orthosis on gait biomechanical characteristics of paretic and non-paretic limbs in hemiplegic patients with genu recurvatum," *Clinical Biomechanics*, vol. 28, no. 1, pp. 73–78, 2013.

[25] J. E. Colgate and G. G. Schenkel, "Passivity of a class of sampled-data systems: Application to haptic interfaces," *Journal of robotic systems*, vol. 14, no. 1, pp. 37–47, 1997.

[26] R. Ortega, A. J. Van Der Schaft, I. Mareels, and B. Maschke, "Putting energy back in control," *IEEE Control Systems Magazine*, vol. 21, no. 2, pp. 18–33, 2001.

[27] R. Ortega, A. Van Der Schaft, B. Maschke, and G. Escobar, "Interconnection and damping assignment passivity-based control of port-controlled hamiltonian systems," *Automatica*, vol. 38, no. 4, pp. 585–596, 2002.